# Resolved-detrimental surface crystallization in yttrium lanthanum gallate glasses for optical fiber applications

Florian Calzavara, Pierre Florian, Franck Fayon, Vincent Sarou-Kanian, Théo Guérineau, Sylvain Danto, Younès Messaddeq, Marc Dussauze, Veronique Jubera, Thierry Cardinal, et al.

# Resolved-detrimental surface crystallization in yttrium lanthanum gallate glasses for optical fiber applications

Florian Calzavara[a], Pierre Florian[b], Franck Fayon[b], Vincent Sarou-Kanian[b], Théo Guérineau[c], Sylvain Danto[a] , Younès Messaddeq[c] , Marc Dussauze[d], Véronique Jubera[a], Thierry Cardinal[a*], Evelyne Fargin[a]

[a] Institut de Chimie de la Matière Condensée de Bordeaux, Université de Bordeaux, 87 Avenue du Dr Schweitzer, Pessac F-33608, France

[b] Conditions Extrêmes et Matériaux : Haute Température et Irradiation, UPR 3079, Université d'Orléans, 1 Avenue de la Recherche Scientifique, 45100 Orléans, France

[c] Centre d'optique photonique et laser, Pavillon d'optique et photonique, Université Laval, 2340 rue de la Terrasse, Québec, QC, G1Y2W5, Canada

[d] Institut des Sciences Moléculaires, UMR 5255, Université de Bordeaux, 351 cours de la Libération, Talence Cedex 33405, France

* **Corresponding author:** thierry.cardinal@icmcb.cnrs.fr

**Keywords.** Heavy Metal Oxide glasses, Gallate glasses, Local glass structure, Crystallization, Vibrational Infrared and Raman spectroscopies, Solid-State Nuclear Magnetic Resonance, Optical glass fibers, Infra-Red transparent Materials.

**Abstract.** Gallium-rich Heavy Metal Oxide glasses have become highly attractive optical materials since they exhibit a wide transparency window spanning from the ultraviolet ~ 270 nm up to the mid-infrared region ~6 µm making them promising for a future integration in optical fiber devices. Nonetheless, in most composition, surface crystallization is a key limiting factor for optical fiber drawing using the classical preform-to-fiber method. Herein, taking advantage of structural information from vibrational spectroscopies (Raman/Infrared) and $^{71}$Ga Solid-State Nuclear Magnetic Resonance, we describe the key role of Lanthanum and Yttrium rare – earth elements on the glass structure and their impact on the capability to draw those new glass compositions into optical fibers. This approach emphasizes that Yttrium ions as compared with Lanthanum ones favor the glass disorder, increasing significantly the fraction of $GaO_5$ units with respect to $GaO_4$. That, combined with thermal analysis and examination of the crystallization behaviors, highlight that $Y_2O_3$ prevents the glass devitrification during the glass shaping. The smaller Yttrium radius is believed to be the key physical parameter preventing the precipitation of the $Ba_yGa_{5-y}Ge_{y+1}La_{3-y}O_{14}$ (y= 0, 1, 2, 3) langasite-type crystal phase. This study remains particularly relevant and opens up the way for the development of highly robust power scaled fiber devices operating from the visible up to the challenging mid-infrared domain.

**Graphical abstract.**

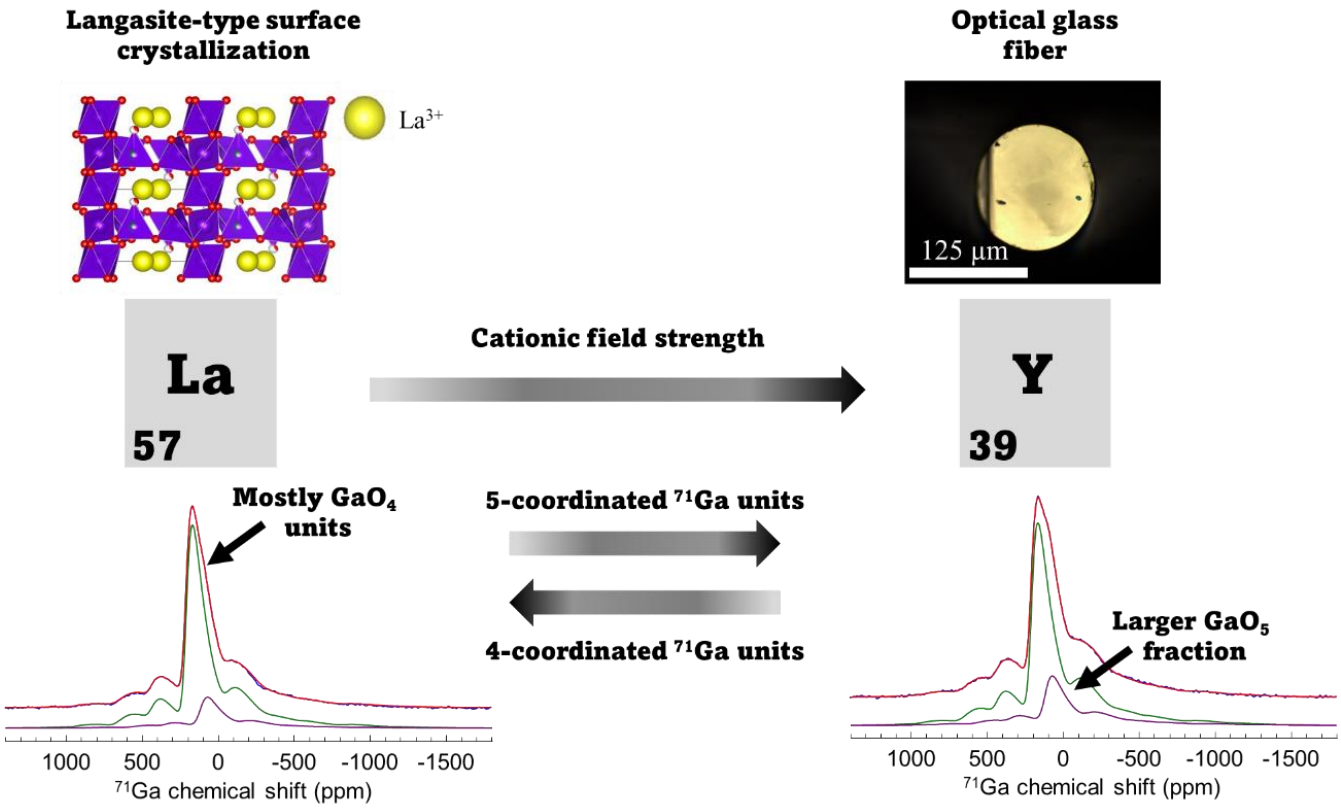

## 1. Introduction.

Since Charles Kao's pioneering work in 1966 [1] pointing out to the ability to guide light throughout a dielectric medium, glass scientists worldwide have focused their efforts on the ability to reduce the optical propagation losses in glass-based light waveguiding technology including notably optical glass fibers. In the following years to the current days, the community has mainly worked with the well-known oxide-based silica glasses since it exhibits extraordinary assets in terms of easy-handling, remarkable stability with respect to devitrification as well as exhibiting superior physical properties. Nonetheless, silica – based glasses are limited in terms of infrared (IR) transparency up to ~ 2 – 3 µm and rare – earth solubility ~ $10^{19}$ ion.cm$^{-3}$ [2] whereas the actual key challenges are based on designing new infrared active or passive light-guiding photonic materials [3], [4] operating in the challenging 3 – 5 µm domain since a wide range of fields can be covered in this spectral window such as health (endoscopes), biology, defense and security (remote sensing using IR spectroscopic imaging and analysis) [5]. Thereby, new glass compositions need to be alternatively explored to substitute to silica glasses. Chalcogenide- and fluoride- based glasses are now known materials capable of providing a large panel of applications in the near- and mid- infrared spectral region. However, their poor thermal resistance and their weak mechanical robustness may limit their use as compared to robust oxide-based glasses. In comparison with the chalcogenide and fluoride IR materials, germano – gallate ($GeO_2$-, $Ga_2O_3$)-oxide glasses exhibit high thermal properties and superior mechanical hardness [6], [7] while providing an extended infrared transmission window up to ~ 5.5 - 6 µm. However even if those glasses present superior assets, the current major challenge consists in extending gallium-rich glass compositions while preventing the glass devitrification during the glass shaping using the classical preform-to-fiber approach. Indeed, the glass preform is often kept at a temperature close to the beginning of the crystallization temperature during the fiber fabrication thus favoring the nucleation and growth of crystalline phases. In order to overcome those significant challenges, glass scientists concentrate their efforts in managing key parameters including glass composition with adapted viscosity and drawing process technologies.

In terms of devitrification challenge, we have shown in our previous studies [8] that the introduction of low field strength cations (defined as the ratio CFS = $Z^+_i / r^2_i$ where $Z^+$ and r are the charge and the ionic radius of the cation i respectively) in the system $Ga_2O_3 – GeO_2 –$ BaO favors the surface crystallization of zeolite-type phase, thereby preventing the optical fiber drawing [9], [10]. We have proposed that such behavior is favored by the thermal mobility of

the small ionic radius cations such as sodium or potassium. By contrast, we have further recently shown based on the study of Wen *et. al* [11] that the introduction of an equimolar mixed ratio of high field cation such as lanthanum and yttrium rare – earth elements prevent the devitrification phenomenon [12].

We propose herein to investigate the role played by lanthanum and yttrium ions onto the crystallization behaviors and the glass properties of a selected germano – gallate composition. This study aims to provide the most appropriate ratio $YO_{3/2}$:$LaO_{3/2}$ limiting at best the glass devitrification, for the development of mid-infrared transparent gallium-based HMO glass optical fibers using the classic preform-to-fiber approach.

## 2. Experimental section.

**2.1. Glass synthesis.** Glasses were prepared by the conventional melt-quenching technique from high purity raw precursors such as gallium oxide $Ga_2O_3$ (99.999 %, Stream chemical), germanium oxide $GeO_2$ (99.999 %, Fox Chemicals), barium carbonate $BaCO_3$ (99.95 %, Alpha Aesar), yttrium oxide (99.99 %, Alpha Aesar) and lanthanum oxide (99.9 %, Sigma Aldrich). The powder precursors were thoroughly mixed in an agate mortar and then placed in a pure platinum crucible for a decarbonation treatment at 950°C for 1 hour. They were then melted under ambient atmosphere at atmospheric pressure in the open Pt crucible for ~ 1 – 2 hours before being water quenched. The melting temperature has been increased from 1550°C to 1640°C when the content of yttrium oxide increases. No further annealing treatment was performed on the investigated glasses in order to avoid possible nucleation processes. The samples were then cut and polished on both parallel faces for further optical characterizations. Confirmation of nominal glass stoichiometry have been verified using inductively-coupled plasma optical emission spectroscopy measurements on several glass compositions with a deviation of ± 2 at %. The amorphous state on all the glass samples has been verified using X-Ray Diffraction (XRD) from 8.024 ° to 79.985 ° with a step interval equals to 0.017°. The TEM measurements have revealed the absence of phase separation at a nanometric scale on the investigated glass samples.

**2.2. Physical and thermal characterizations.** Thermal properties including the onset of glass transition temperature ($T_g$) and the onset of crystallization ($T_x$) were measured on a Netzsch DSC Pegasus 404 F3 apparatus in a platinum pan using glass powder. A heating rate of 10 °C.min$^{-1}$ has been set for the study of the characteristic temperatures. The onset of $T_g$ and $T_x$ were determined from the DSC trace from the tangents crossing. The error has been estimated

to be equal to ± 2°C. The viscosity in the interval of $10^{10}$ to $10^{7.5}$ Poise was recorded on a Theta US parallel plate viscometer, on a ~10 mm diameter and ~ 6 - 8 mm height cylindrical samples placed between two silica spacers. The samples, under a 300 g charge, were heated up to 700 °C with a heating rate of 5 °C.min$^{-1}$ and then up to 850 °C with a heating rate of 2 °C min$^{-1}$. The potential fiber drawing temperature was estimated for a viscosity between $10^{5.5}$ and $10^{6.5}$ Poise by a linear extrapolation of the viscosity curve with an approximated error of ± 5 °C. In this approach, we assumed a linear behavior of the logarithm of the viscosity versus the temperature curve in this regime of viscosity according to the Arrhenius law stating that $\ln(\eta(T)) = E_\eta\ R^{-1}\ T^{-1}$ in which $\eta$ is the glass viscosity, $E_\eta$ the viscosity's activation energy (kJ.mol$^{-1}$), R the gas constant (kJ.mol$^{-1}$.K$^{-1}$) and T the temperature (K). The density $\rho$ was obtained from the average of five measurements per sample using Archimedes' method by immerging a glass chunk in diethyl phthalate at room temperature on a Precisa XT 220A weighing scale. The estimated errors were around ± 0.01 g.cm$^{-3}$. The Knoop microhardness (HK) measurements were carried out using a Leica WMHT Auto Apparatus equipped with a charge coupled device (CCD) camera. A charge of 100 g (= 0.981 N) was applied during 20 seconds. Ten measurements performed on the sample surface were averaged in order to obtain the Knoop microhardness of the glass.

**2.3. Structural characterizations.** Unpolarized Raman spectra were recorded with a confocal micro-Raman spectrometer LabRAM HR Evolution (Horiba Jobin Yvon) equipped with a Synapse CCD detector cooled down to -70 °C using a 532-nm radiation from a diode pumped solid state laser (output power = 20 mW). The incident laser beam was focused onto the sample through a microscope with a 50x objective (NA = 0.50, Olympus). Scattered light was dispersed by 600 grooves. mm$^{-1}$ grating system. Raman spectra have been recorded from 200 cm$^{-1}$ to 1500 cm$^{-1}$. They were further corrected by the Bose-Einstein factor. Reflectance infrared spectra have been recorded with an incident angle of 11° from 200 to 1500 cm$^{-1}$ with a spectral resolution of 4 cm$^{-1}$ using a Fourier Transform Spectrometer Vertex 70 V. A mid-infrared source has been used (globar type). All measurements were performed in vacuum. The spectra have been averaged from over 200 scans. Kramers-Kronig transforms have been performed in order to extract the optical constants $n_0$ and k from the complex refractive index $\underline{n}$ equals to $\underline{n} = n_0 + i\ k$.

$^{71}$Ga solid-state NMR spectra were obtained on a wide bore 20.0 T Bruker Neo spectrometer using a rotor-synchronized solid echo excitation with a full echo acquisition (i.e. $T_{90} - \tau - T_{90}$ – acq.) to avoid any ambiguity related to phasing and baseline correction. All powdered samples

have been packed in 1.3 mm zirconia rotors, spun at 64.0 kHz and the τ delay set to 12 rotor periods (i.e. 187 µs). A short, selective, pulse $T_{90}$ of 0.9 µs has been used at a radio-frequency field of 100 kHz ensuring a full excitation of the spectra. A recycle delays were 0.5 s (spin-lattice relaxation times estimated ≤ 100 ms) and 16384 transients were accumulated for all compositions. $^{71}Ga$ chemical shift is referenced to a 1M solution of $Ga(NO_3)$. All spectra were simulated using DMFit based on the so-called Czjzek (or Gaussian Isotropic) model rendering the central <1/2,-1/2> transition in the finite spinning-speed regime (i.e. taking into account its spinning sidebands) [13].

**2.4. Crystallization studies.** The investigated glasses have been crushed into powder in order to undergo a strictly identical thermal treatment. Powders were first placed in the same furnace on a platinum cover. Powders have been then heated up to the crystallization temperature $T_x$ + 10°C for 12 hours with a heating rate equals to 2°C.min$^{-1}$. Samples have been subsequently cooled down to 400 °C with a rate equal to 5°C.min$^{-1}$. No color change has been observed at the end of the thermal treatment. X-Ray Diffraction (XRD) has been then performed from 8.024 ° to 79.985 ° with a step interval equals to 0.017°.

**2.5 Optical properties.** Optical properties have been investigated by transmission measurements. The infrared transmission spectra were recorded on a spectrometer Brüker Equinox 55 with a spectral resolution of 4 cm$^{-1}$. The spectra have been recorded from an average of 32 scans. The ultraviolet– visible transmission spectra were recorded on a Cary5000 (Varian) from 200 nm to 2500 nm with a spectral resolution of 1 nm. The refractive indices were measured by prism coupling on a M-line 2010/M Metricon apparatus at 532 nm, 633 nm, 972 nm, 1308 nm and 1538 nm with an estimated error of ± 0.005. The chromatic dispersion has been obtained while fitting the measured refractive indices using the well-known Sellmeir equation $n^2 = 1+ (A_1 \lambda^2) (\lambda^2 - B_1)^{-1} + (A_2 \lambda^2) (\lambda^2 - B_2)^{-1}$ where $A_i$ and $B_i$ are the Sellmeir coefficients and λ the wavelength (nm).

**2.5. Optical fiber drawing experiments.** Glass preforms were prepared using the conventional melt-quenching technique according to the heating protocol presented in **Section 2.1**. The melts were casted into a 10 millimeter diameter pre-heated stainless mold before being placed in an annealing furnace at $T_g$ - 40 °C during 4 hours in order to reduce the internal mechanical stress. Piece of ~1 cm length from the glass preforms were cut and polished on both parallel faces for further optical characterizations. The glass preforms were drawn using dedicated optical fiber drawing towers. The tower is equipped with furnace having a sharp temperature profile, a

diameter and tension controllers, a collecting drum. The heating chamber is kept under continuous dry argon gas flow (2 $mL.min^{-1}$). Preforms are fed into the furnace and the temperature is gradually increased with the rigorously same heating rate up to the fiber's drawing temperature, that is a gradually increase of the temperature of ~ 20°C.$min^{-1}$ up to ~ $T_g$ - 40°C. Then the furnace temperature was increased with a ramp of ~ 10°C.$min^{-1}$ until the bottom-section of the preform is locally softened then forming a drop, falling down by gravity until being hooked to the collecting drum system (drum velocity: ~ 0.5 $m.min^{-1}$, preform feed rate: ~ 0.5 $mm.min^{-1}$ ).

## 3. Results and discussion.

**3.1. Glass compositions.** The investigated glass compositions explored using the classical melt-quenching technique are reported in **Table 1**. The selected compositions are 40.00 $GaO_{3/2}$ – 26.43 $GeO_2$ – 16.43 BaO – x $YO_{3/2}$ – (17.14 – x) $LaO_{3/2}$ with x = 0, 8.57, 12.86 and 17.14, respectively labelled as "17 $LaO_{3/2}$", "8.5 $YO_{3/2}$ – 8.5 $LaO_{3/2}$", "13 $YO_{3/2}$ – 4 $LaO_{3/2}$" and "17 $YO_{3/2}$". The pseudo ternary phase diagram presented in **Figure 1** displays the studied glasses in the multi-component system $GaO_{3/2}$ – $GeO_2$ – BaO – $REO_{3/2}$ (RE = Y, La). A few known germanate and gallate crystalline phases containing either rare – earth elements (Lanthanum or Yttrium) or only barium oxide are also displayed. Nearby our investigated glass composition, one can observe the presence of the crystalline langasite-type solid solution $Ba_yGa_{5-y}Ge_{y+1}La_{3-y}O_{14}$ phases with y = 0, 1, 2, 3. To the best of our knowledge, no yttrium-containing phase is found next to our selected compositions. The main relationships between the crystallization behavior and the structural features depending on the ratio $YO_{3/2}$:$LaO_{3/2}$ as well as the thermal and the optical properties were further studied while keeping fixed the glass network former ratio $R$ = $GaO_{3/2}$:$GeO_2$ equals to 1.5 and the amount of barium oxide. The theoretical glass compositions explored using the classical melt-quenching techniques are reported in **Table 1.**

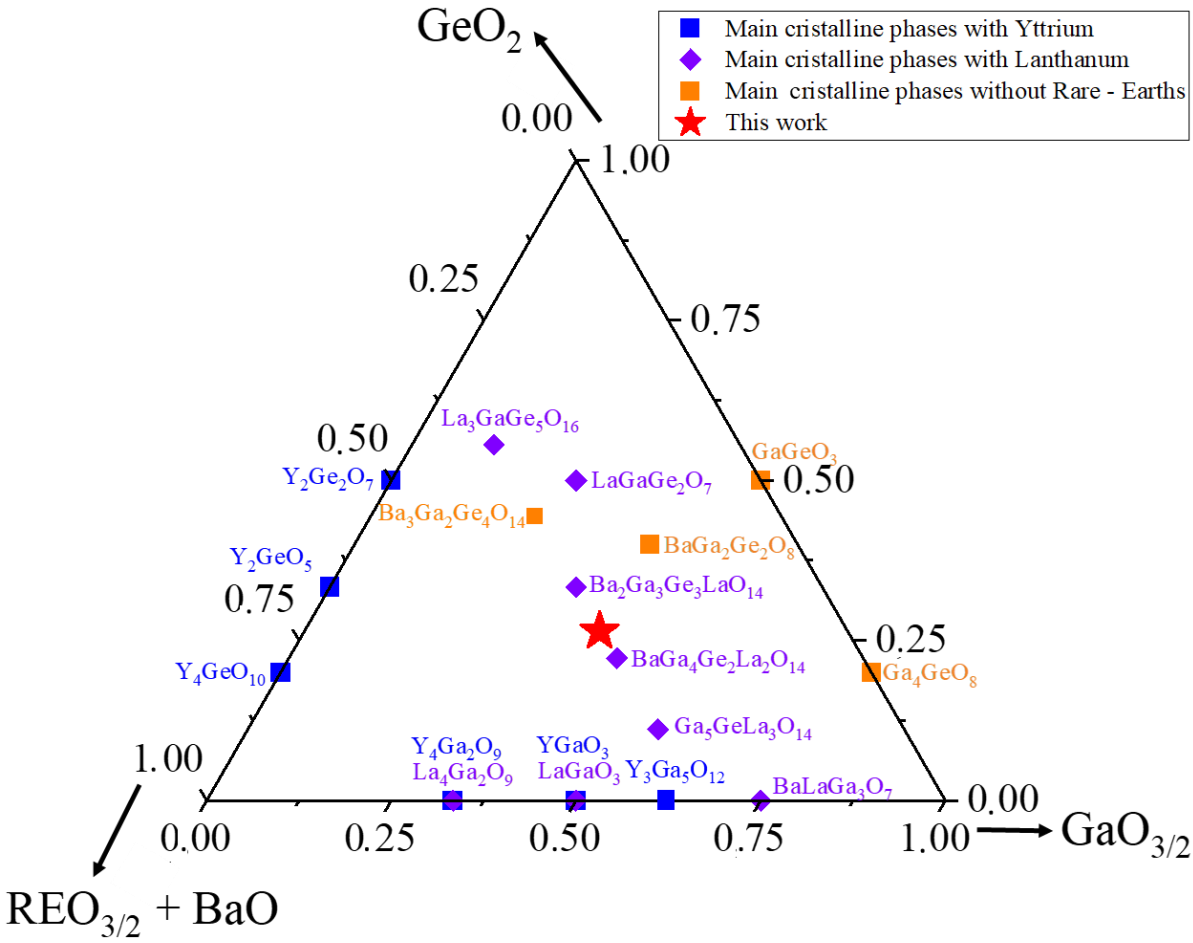


**Figure 1 : $GaO_{3/2}$ – $GeO_2$ – (BaO + $REO_{3/2}$) (RE = La, Y) pseudo – ternary diagram. Our investigated glass composition (*i.e.* 40 $GaO_{3/2}$ – 26.43 $GeO_2$ – 16.43 BaO – 17.14 $REO_{3/2}$) is represented by a red star. The main crystalline phases are presented in blue, purple and orange items.**

**Table 1: Labels and theoretical glass compositions of the investigated glass series .**

| | Composition (mol %) | | | | | Composition (cationic mol %) | | | | |
|---|---|---|---|---|---|---|---|---|---|---|
| | $Ga_2O_3$ | $GeO_2$ | BaO | $La_2O_3$ | $Y_2O_3$ | $GaO_{3/2}$ | $GeO_2$ | BaO | $LaO_{3/2}$ | $YO_{3/2}$ |
| **17 $LaO_{3/2}$** | 28.00 | 37.00 | 23.00 | 12.00 | 0.00 | 40.00 | 26.43 | 16.43 | 17.14 | 0.00 |
| **8.5 $LaO_{3/2}$ – 8.5 $YO_{3/2}$** | 28.00 | 37.00 | 23.00 | 6.00 | 6.00 | 40.00 | 26.43 | 16.43 | 8.57 | 8.57 |
| **4 $LaO_{3/2}$ – 13 $YO_{3/2}$** | 28.00 | 37.00 | 23.00 | 3.00 | 9.00 | 40.00 | 26.43 | 16.43 | 4.29 | 12.86 |
| **17 $YO_{3/2}$** | 28.00 | 37.00 | 23.00 | 0.00 | 12 | 40.00 | 26.43 | 16.43 | 0.00 | 17.14 |

**3.2. Optical glass fibers.** Drawing experiments using the protocol described in **Section 2.5** were first conducted on the 17 $LaO_{3/2}$ preform. As shown in the inset of the **Figure 2**, surface crystallization appears on the droplet, preventing further optical fiber shaping. The crystallites

appearing on the glass surface were identified using XRD technique. They were subsequently assigned to langasite-type (LGS) solid solutions $Ba_yGa_{5-y}Ge_{y+1}La_{3-y}O_{14}$ as shown in **Figure 2** (JCPDS cards are 001-072-2464, 00-044-0424, 00-041-0348 for y = 0, 2, 3 respectively. No JCPDS card was found for y= 1 crystalline phase). This assignment has been also confirmed by comparing the experimental reflections measured on the glass preform to the synthesized crystal langasite-type phases for y = 0 up to y = 3.

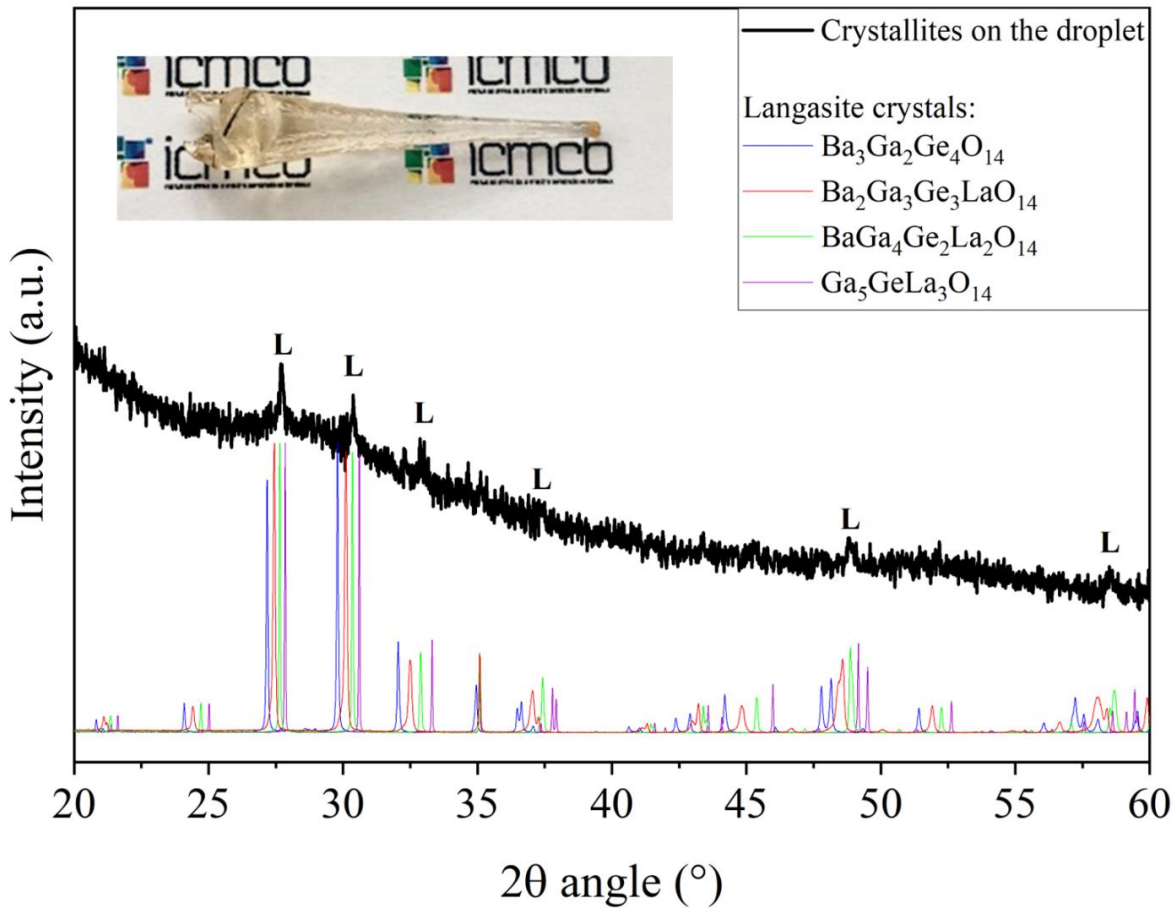


**<u>Figure 2:</u> (a) XRD pattern obtained from crystallites on the droplet. Assignations reveals the characteristic reflections of the langasite $Ba_yGa_{5-y}Ge_{y+1}La_{3-y}O_{14}$ langasite-type solid solution. The droplet of the 17 $LaO_{3/2}$ sample displaying crystallites at the surface is shown in inset.**

LGS structure belongs to the structure type of calcium germanate $Ca_3Ga_2Ge_4O_{14}$ with the space group P321 (n150) in the chemical formula $A_3BC_3D_2O_{14}$ where A and B cations are respectively located on decahedral site (3e) and octahedral site (1a). C and D, on the other hand, are located in tetrahedral site respectively 3f and 2d Wyckoff's positions [14]. As shown in **Figure 3a** displaying the langasite-type crystal $Ga_5GeLa_3O_{14}$, LGS form a layered structure of (Ga, Ge)$O_4$ tetrahedra perpendicular to the crystallographic c-axis connected through their vertices. These

layers are connected by octahedrally coordinated (Ga, Ge) ions (site B, 1a) and highly coordinated $La^{3+}$ or $Ba^{2+}$ ions when appropriate (site A, 3e). The remaining tetrahedral sites of the langasite structure are being occupied by either gallium or germanium cations (site C and D, 2d, 3f).

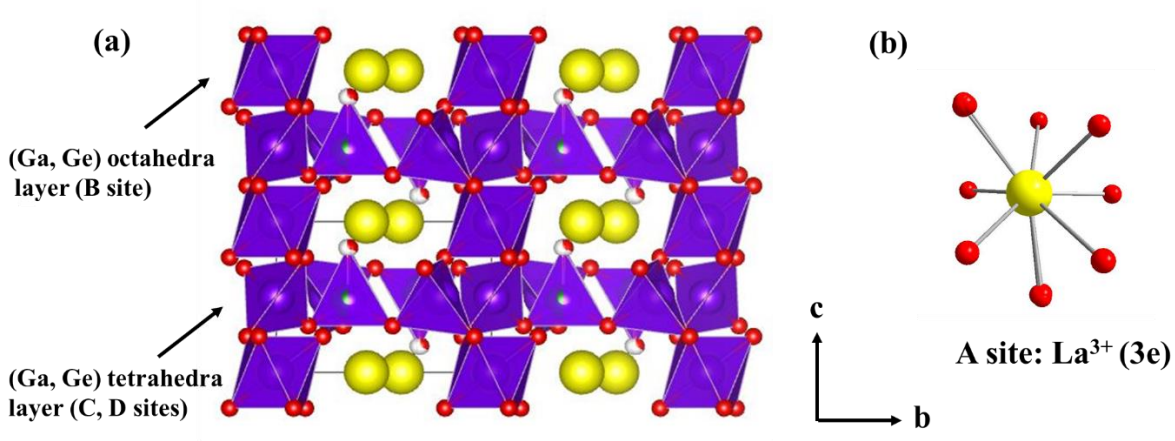


**Figure 3: Crystal structure of the langasite-type crystal phase $Ba_yGa_{5-y}Ge_{y+1}La_{3-y}O_{14}$ with y= 0. (b) The discussed critical A site occupied by Lanthanum ions is displayed in inset.**

Besides, similar drawing experiments were first conducted on the 17 $YO_{3/2}$-preform. As shown in the inset of **Figure 4** displaying a fiber section, successful glass shaping was obtained for the $YO_{3/2}$-rich sample in which ~ 10 – 12 of meters with a diameter ranging from ~ 100 - 300 µm. Here it is noteworthy to remember that the ability to extend the glass composition "8.5 $YO_{3/2}$ – 8.5 $LaO_{3/2}$" has already been demonstrated elsewhere with losses about 6 $dB.m^{-1}$ at 1310 nm [12]. The key feature here in order to explain the absence of devitrification with the $YO_{3/2}$-sample relies on the A site occupied by the highly coordinated Barium and Lanthanum cations. Indeed, the previously reported langasite-type crystalline families such as several gallate germanium-containing or even their gallate silicon-containing analogues $TR_3Ga_5M^{4+}O_{14}$ (M= Si, Ge) in which those crystalline phases were indexed only with a cation exhibiting a relatively large ionic radius such as La, Nd or Pr [15]. Therefore, the lack of known Yttrium-containing structures suggests that small radius of Yttrium cations is believed to be the key enabling to prevent the langasite-type precipitation during the glass shaping. This assumption will be examined through further studies including the crystallization behaviors in the next subsections.

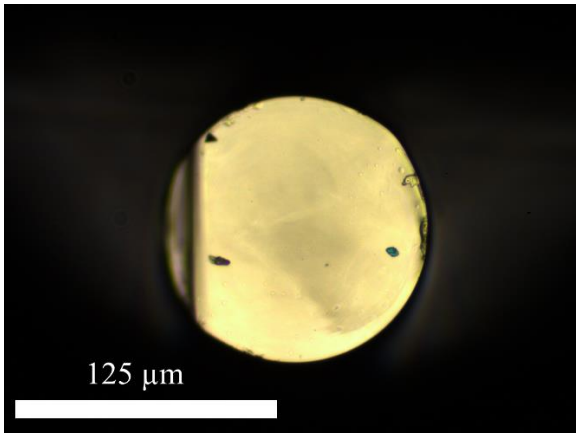


**Figure 4: An optical photography of the fiber section.**

**3.3. Thermal and rheological properties.** The understanding of the ability to compositionally extend optical glass material remains tricky since the crystallization processes that could occur while heating the glass preform close to the onset of the crystallization temperature remains complex and are still not yet fully understood. The study of the fundamental glass properties can be considered as a good starting point to extend the $YO_{3/2}$-containing glass compositions as optical fibers. We first focus onto the key properties such as the glass viscosity $\eta(T)$, the characteristic thermal temperatures $T_g$ and $T_x$ as well as the glass packing density $\rho$. The evolution of the logarithm of the viscosity with respect to the temperature is presented in **Figure 5a.** One observes that for a fixed temperature, the glass viscosity increases when the yttrium content increases, as well as the potential fiber drawing temperature $T_{drawing}$ estimated for a viscosity $\eta$ value ranging from 5.5 and 6.5 Poises. Such changes suggest important variations in terms of thermal and physical properties. Those ones are regrouped in **Table 2** and are displayed in **Figure 5b-d**. In terms of glass transition temperature variations, one notices that the introduction of yttrium oxide with respect to lanthanum oxide leads to increase linearly the $T_g$ values from 729 °C up to 746 °C as shown in **Figure 5b**. Nonlinear behavior on the molar volume depending on the content of $YO_{3/2}$ is observed as displayed in **Figure 5d.** The compactness drastically increases for $YO_{3/2}$ content above 8.5 mol %, traducing most probably a structural change of the glass network for high yttrium loading.

Regarding now the crystallization peaks obtained from the DSC thermal measurements in **Figure 5c**, one can observe that introducing Yttrium oxide within the glass matrix results in shifting significantly the maximum of the crystallization peak of 60 – 70 °C. This indicates important changes in the crystallization behavior of the $YO_{3/2}$-containing glasses as compared to the lanthanum one. In addition to that, one notices in the inset of the **Figure 5** displaying the

derivative of the $YO_{3/2}$- and $LaO_{3/2}$-thermograms that the substitution of lanthanum by yttrium ions involves a diminution of the slope of the derivative curve. This strongly suggests a less pronounced devitrification behavior for the $YO_{3/2}$-rich sample. In addition to that, one can also see that the Knoop micro – hardness is slightly greater for the yttrium containing glass as compared to the lanthanum one. Such evolution in the glass properties according to the $YO_{3/2}$ content may suggest variations in the crystallization behavior as well as local glass structure changes. This statement will be respectively discussed in the **Section 3.4** and **Section 3.5.**

**Table 2 : Thermal and physical properties of the investigated glass series.**

| **Name** | $T_g$ (± 2°C) | $T_x$ (± 2°C) | $\Delta T$ (± 4°C) | $\rho$ ± 0.01 ($g.cm^{-3}$) | $V_m$ ± 0.06 ($cm^3.mol^{-1}$) | $T_{drawing}$ **range** (°C) | $H_K$ (GPa) |
|---|---|---|---|---|---|---|---|
| **17 $LaO_{3/2}$** | 729 | 846 | 117 | 5.19 | 31.90 | 832 - 851 | 5.5 |
| **8.5 $LaO_{3/2}$ – 8.5 $YO_{3/2}$** | 739 | 886 | 147 | 5.13 | 31.10 | 855 - 875 | - |
| **13 $YO_{3/2}$ – 4 $LaO_{3/2}$** | 741 | 890 | 149 | 5.04 | 31.06 | 859 - 879 | - |
| **17 $YO_{3/2}$** | 746 | 896 | 150 | 4.96 | 30.96 | 870 - 889 | 6.0 |

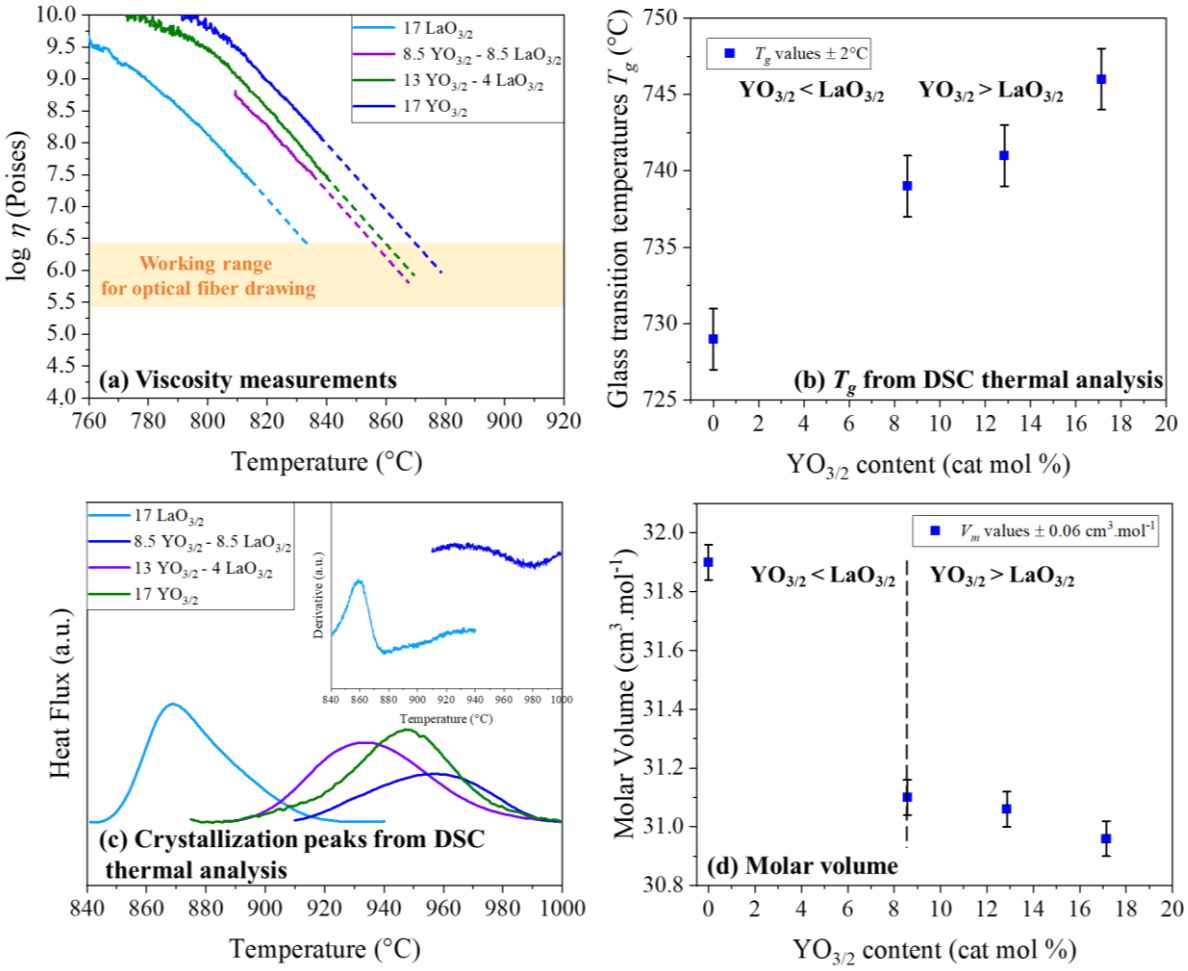


**Figure 5: (a) Logarithm of the viscosity *η(T)* with respect to the temperature. Here one notes that the dashed linear lines have been extrapolated from the solid lines which correspond to the viscosity measurement - (b) the nonlinear evolution of the glass transition temperatures $T_g$ - (c) the evolution of the crystallization peaks depending on the $YO_{3/2}$ content. The derivative of the 17 $YO_{3/2}$ and the 17 $LaO_{3/2}$ is shown in inset - (d) the nonlinear evolution molar volume $V_m$ with respect to the $YO_{3/2}$ content.**

**3.3. Crystallization behaviors.** The XRD patterns obtained after the thermal treatment presented in **Section 2.4** are presented in **Figure 6**. For $LaO_{3/2}$-containing glasses, one observes mainly the appearance of the langasite-type solid solution even when the amount of yttrium oxide is greater than lanthanum oxide. Besides, high amount of Yttrium oxide seems to favor the precipitation of crystalline $Y_3Ga_5O_{12}$ phase (PDF card 01-073-1374). The remaining diffraction peaks could not be clearly assigned here for the 17 $YO_{3/2}$-sample. Herein, the key points lie on *(i)* the broadening of the full half width maximum (FWHM) of the XRD pattern upon the introduction of $YO_{3/2}$ and *(ii)* the non-formation of the langasite-type phase with the

$LaO_{3/2}$-free sample. The first item points clearly to a reduction of the langasite-type crystallite sizes upon the introduction of $YO_{3/2}$. The second item signifies that the formation of langasite-type crystalline phase in which the A site is occupied by a smaller ionic radius rare earth is not favored. Those crystallization behaviors explain the role of Yttrium oxide in limiting the langasite-type crystal formation, enabling fiber drawing of $YO_{3/2}$-rich samples. Such changes in the appearing crystalline phases depending on the rare-earth (La, Y) may also indicate a change in the local glass structure. This will be further examined in **Section 3.5**.

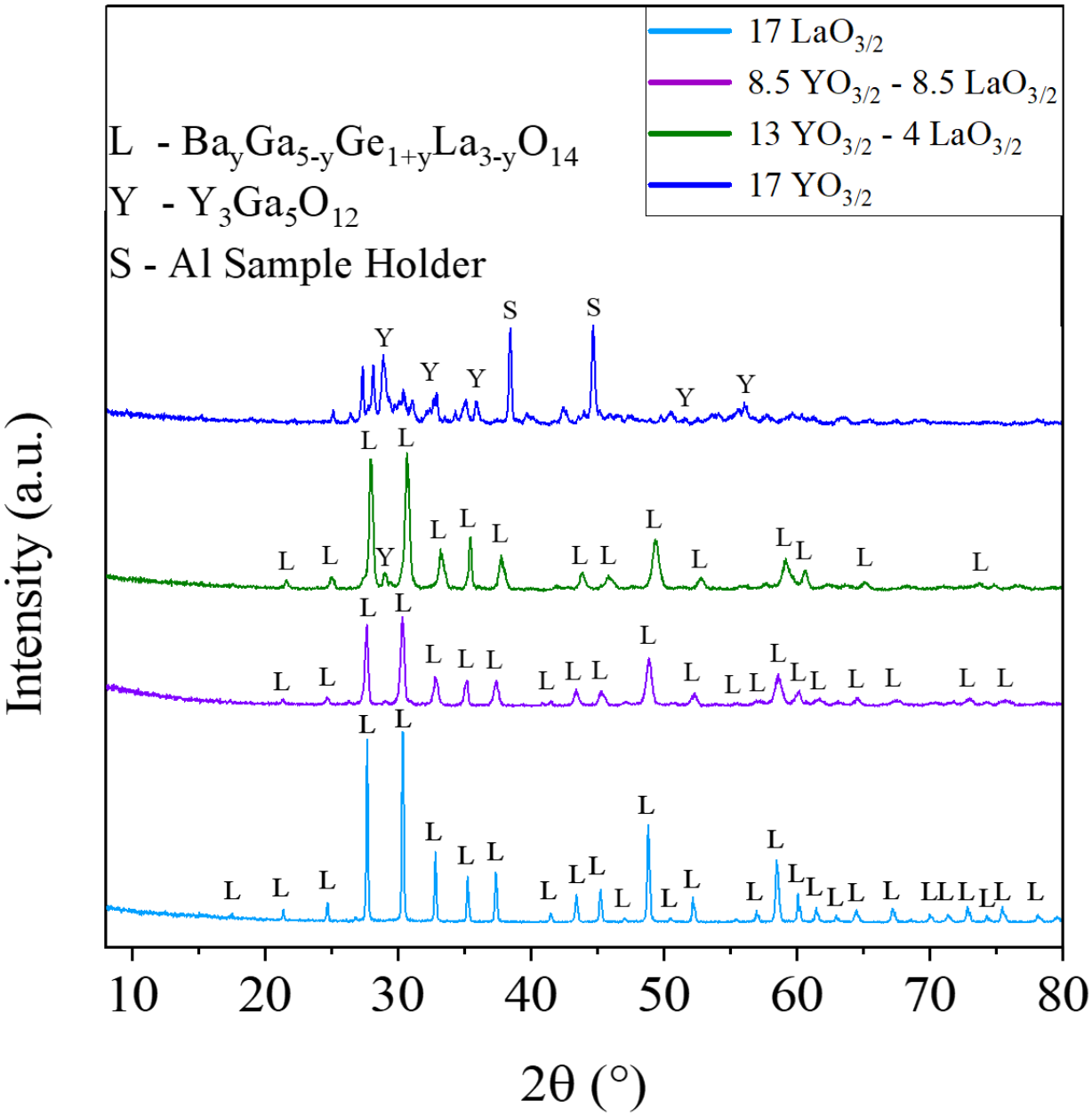


**<u>Figure 6:</u> X-Ray Diffraction pattern (XRD) obtained after the heat treatment of the investigated glasses.**

**3.4. Optical properties.** Gallium-rich germanate materials are remarkably interesting due to their superior optical properties as compared to silica-based optical glasses. Indeed, they exhibit higher refractive indices and longer IR transmission edge up to ~ 5.5 µm. The chromatic dispersions of the optical glasses "17 $LaO_{3/2}$" and "17 $YO_{3/2}$" are presented in **Figure 7a**. One observes that the $LaO_{3/2}$-rich glass exhibit a higher refractive index about ~$10^{-2}$ as compared to the $YO_{3/2}$-rich sample over the studied wavelength range. This slight increase could be assigned to the higher electronic density around Lanthanum ions. The absorption coefficient $\alpha$ is then plotted in **Figure 7b**. One notices that all glass samples are transparent up to ~ 6 µm for an absorption coefficient $\alpha$ = 10 $cm^{-1}$. In addition, we report in the inset of the **Figure 7b** a characteristic transmission window ranging from the ultraviolet ~ 270 nm up to the mid-IR range of a germano – gallate glasses.

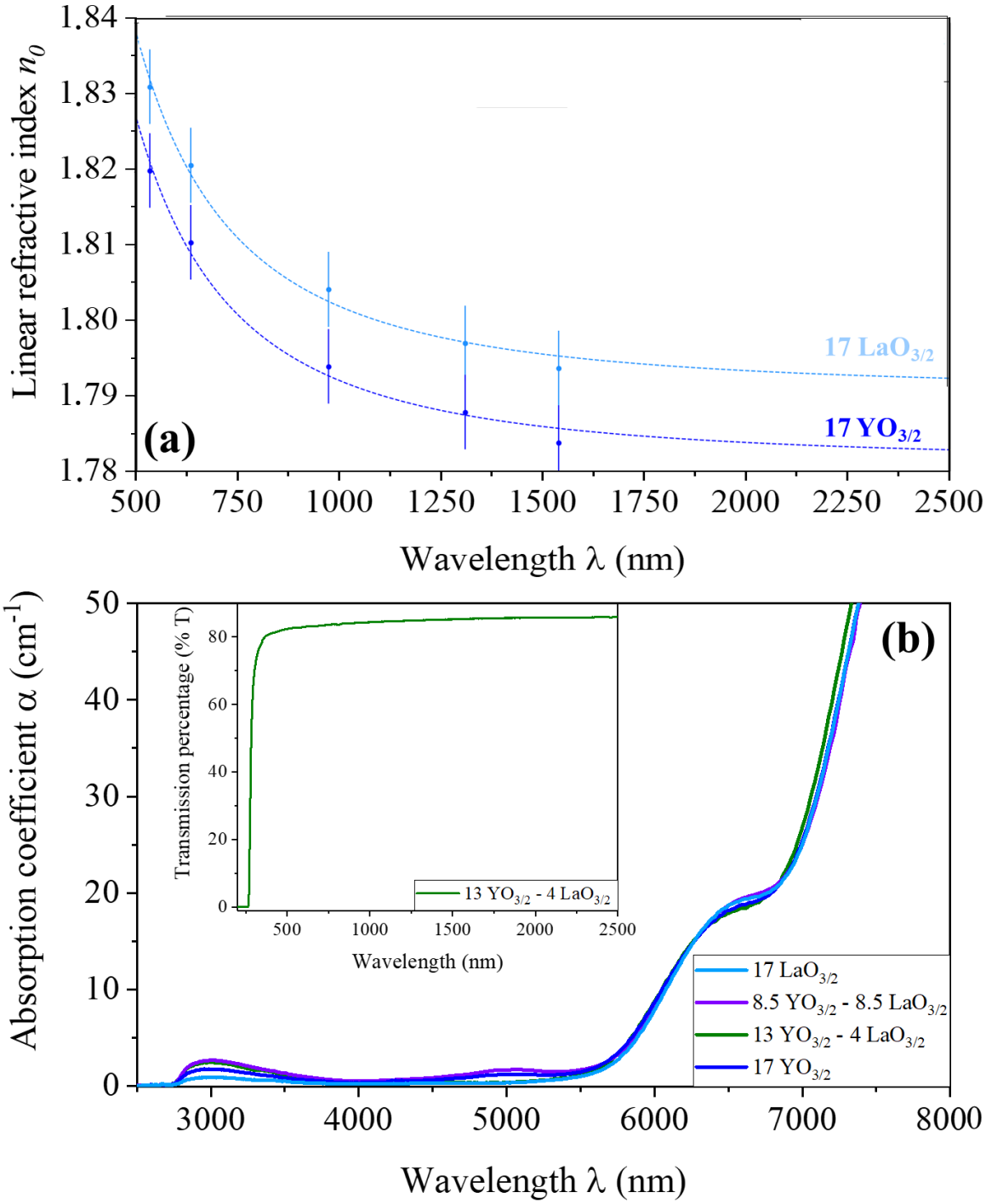


**<u>Figure 7 :</u> (a) Model of the chromatic dispersion of the glass samples labelled "17 $YO_{3/2}$" and "17 $LaO_{3/2}$" and (b) the absorption coefficient in the mid – infrared range from 2500 nm up to 8000 nm for all the investigated glass samples. A transmission spectra is shown in inset.**

**<u>3.4. Structural properties.</u>** The key points for describing the germano – gallate glass network rely mainly on the description of the gallate and germanate interconnected skeleton and in

particular, the study of *(i)* the local gallium environment and its associated charge compensation mechanism and *(ii)* the formation of characteristic $Q_{i\,=\,1,\,2,\,3,\,4}$ germanate units. It is noteworthy here to state that the field strength of each cation in the glass affects significantly its degree of structural disorder of the later. As an illustration and based on previous investigation on analogous glasses such as rare – earth aluminosilicate glasses in the systems $REO_{3/2} – Al_2O_3 – SiO_2$ –based [12], [16]–[18], it has been discussed using NMR spectroscopy that the increase of the CFS has the following consequences: *(i)* a relative increase of the fraction of $AlO_5$ and $AlO_6$ polyhedra, *(ii)* the adherence to Loewenstein's avoidance rule relaxes and the amount of Al – O – Al bridges increases and (*iii*) the preferential amount of Al – O – Al bridges on silicon weakens and Al–NBO species are increasingly formed [16]. In our case, it is expected that gallium cations in germano – gallate glasses behaves like aluminum in alumino – silicate glasses [20], [21]. Therefore, the use of $^{71}$Ga solid-state Nuclear Magnetic Resonance to probe the $^{71}$Ga environment combined with vibrational spectroscopies (Raman/Infrared) to probe the germanate skeleton turns out to be appropriate.

**Solid-State Nuclear Magnetic Resonance spectroscopy.** $^{71}$Ga solid-state Nuclear Magnetic Resonance (SSNMR) spectra collected at high magnetic field and very fast spinning are presented in **Figure 8a**. Spectra were normalized according to the main asymmetric broad peak located around ~214 ppm. Indeed, the asymmetry of the main broad peaks can partially be attributed to a shoulder appearing around ~125 ppm and which intensity increases upon increasing the $YO_{3/2}$ : $LaO_{3/2}$ ratio. In order to better understanding those spectral variations, deconvolution of the characteristic line shapes are presented in **Figure 8b-c** using the Czjzek distribution applicable to half-integer nuclei in isotropically disordered environments. The reader here has to keep in mind that even at the combined fast spinning rates and high magnetic field used here, there is a remaining overlap between the spinning sidebands and the central peak due to the large quadrupolar interaction experienced by $^{71}$Ga. Those ones were taken into account in the Czjzek model function computed here under finite spinning speed assumption. A very satisfactory deconvolution can be obtained using two peaks around ~214 ppm and ~125 ppm which can be respectively assigned to 4- and 5-coordinated gallium units [22]–[24]. It does hence not appear to be necessary to consider the presence of 6- coordinated gallate units to account for the experimental spectra. It can then be seen that the introduction of Yttrium oxide with respect to Lanthanum oxide favors the formation of $GaO_5$ units at the expense of $GaO_4$ units. This results corroborates with previous investigations reported in analogous rare – earth alumino – silicate glasses stating that the structural disorder enhances while increasing

the cationic field strength which results in a larger fraction of higher coordinated aluminate units. In particular, the study of Schaller *et al.* [25] showing that the higher cationic field strength of yttrium as compared with lanthanum cations favors the amount of higher coordinated aluminate species. Moreover the $\sigma_c$ parameter of the "Czjzek" model measures the width of the Gaussian distribution of the quadrupolar tensor arising from bond lengths and bond distance distributions around the observed nuclei and its increase upon increasing $YO_{3/2}$ content hence also confirms the above-mentioned increase in disorder with substitution of La by Y. The fitting SSNMR parameters obtained through the employed model are shown in **Table 4**.

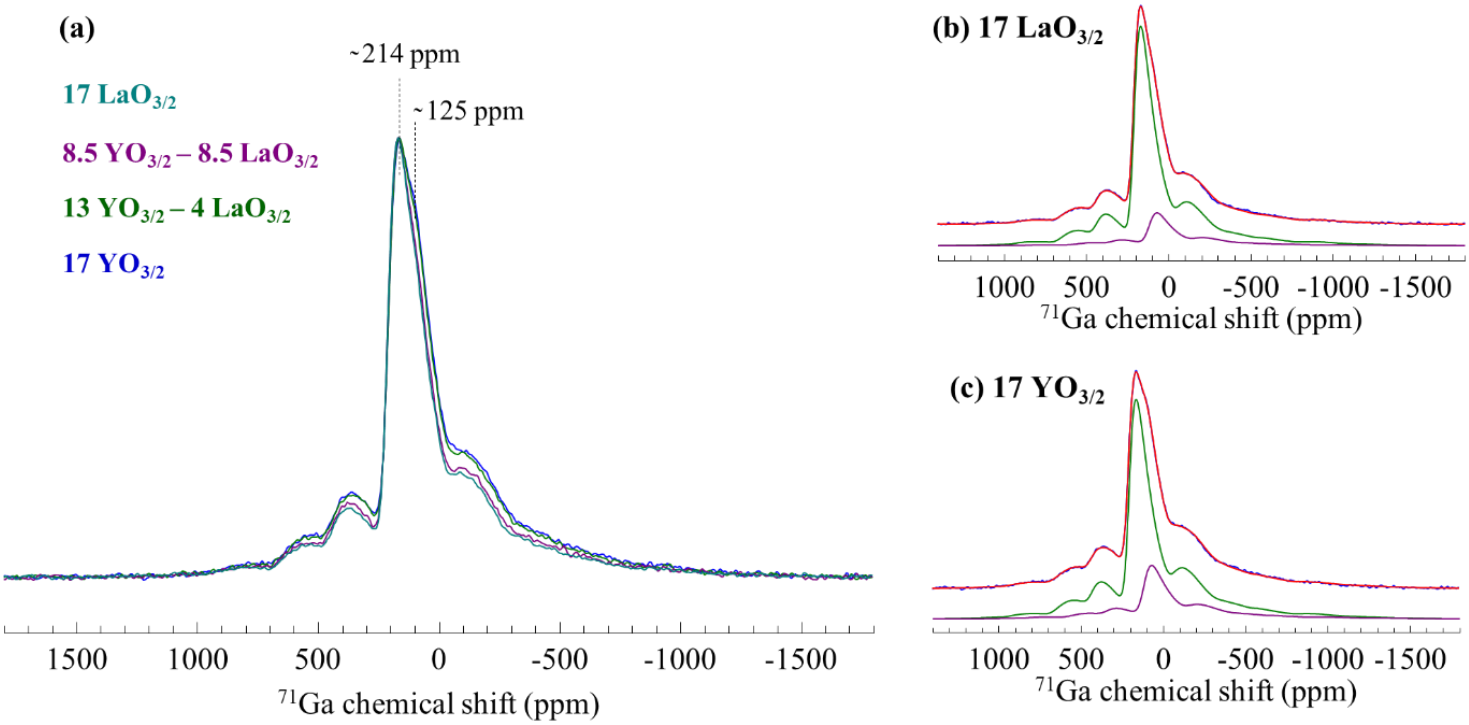


**<u>Figure 8:</u> (a) $^{71}$Ga solid-state Nuclear Magnetic Resonance (SSNMR) spectra of the glass compositions along with the simulation of (b) 17 $YO_{3/2}$ and (c) 17 $LaO_{3/2}$ spectra with the experimental data in blue, the simulation in red, the $GaO_4$ component in green and the $GaO_5$ component in purple.**

**<u>Table 3</u> : Solid-state $^{71}$Ga solid-state Nuclear parameters from line shape fitting of the investigated rare – earth (RE= La, Y) containing germano – gallate glasses**

| Glass sample | Coordination number | Proportion (%) | $\delta_{iso}$ (ppm) | $\Delta\ \delta_{iso}$ (ppm) | $\sigma_C$ |
|---|---|---|---|---|---|
| **17 $LaO_{3/2}$** | 4 | 85 | 215.9 | 50.4 | 9.15 |
| | 5 | 15 | 123.7 | 65.8 | 9.72 |
| **8.5 $YO_{3/2}$ – 8.5 $LaO_{3/2}$** | 4 | 85 | 215.6 | 50.5 | 9.39 |
| | 5 | 15 | 123.6 | 60.1 | 9.71 |
| **13 $YO_{3/2}$ - 4 $LaO_{3/2}$** | 4 | 82 | 213.5 | 52.4 | 9.65 |
| | 5 | 18 | 120.8 | 62.7 | 9.74 |
| **17 $YO_{3/2}$** | 4 | 78 | 213.8 | 51.8 | 9.68 |
| | 5 | 22 | 124.8 | 64.3 | 10.2 |

The evolution of the number fraction of $GaO_4$ and $GaO_5$ units with respect to the cationic molar percent of lanthanum oxide $LaO_{3/2}$ is shown in **Figure 9**. Similarly to the previous behaviors regarding the thermal and physical properties, one observes a nonlinear evolution of the $GaO_4$ and $GaO_5$ units depending on the ratio $YO_{3/2}$:$LaO_{3/2}$.

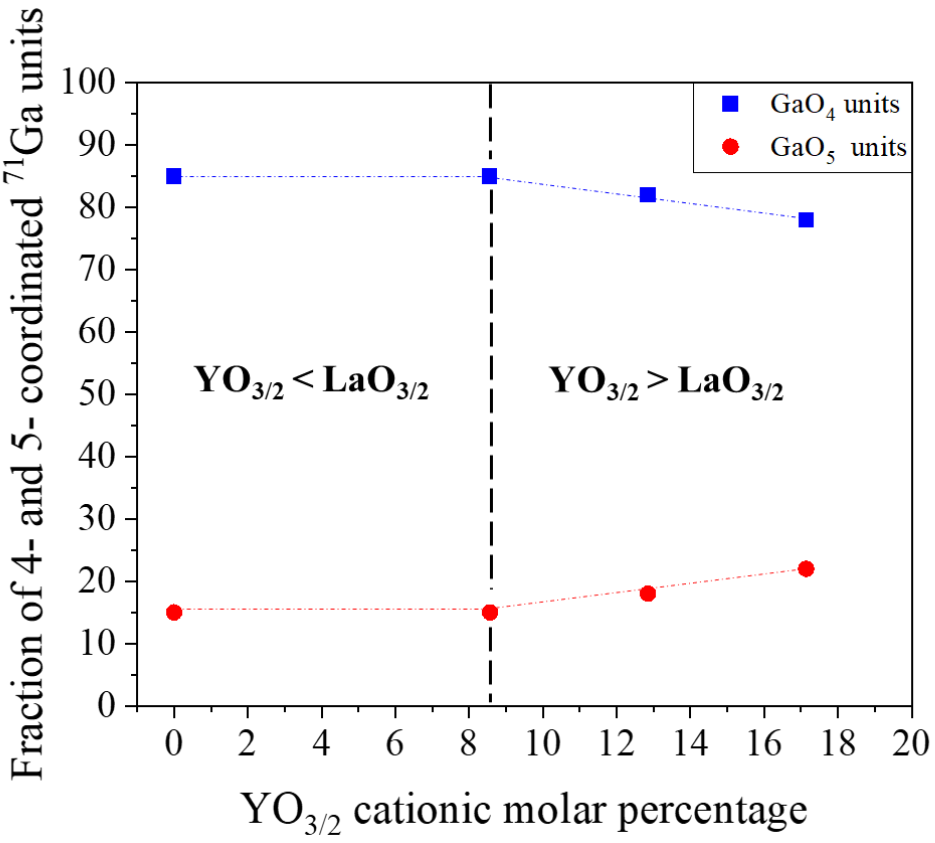


**Figure 9 : Evolution of the number of $GaO_4$ and $GaO_5$ units with respect to $YO_{3/2}$ cationic molar percent. Error bars are integrated in each symbol.**

**Vibrational Raman/IR spectroscopies.** Unpolarized Raman and Fourier Transformed InfraRed (FTIR) spectra of the investigated glass series are respectively presented in **Figure 10a-b**. Those spectra were respectively normalized with respect to the total area. Vibrational spectra can be decomposed in three main regions which correspond respectively to the frequency domains between 200 – 430 $cm^{-1}$, 430 – 600 $cm^{-1}$ and 600 – 1000 $cm^{-1}$. The lowermost 200 – 430 $cm^{-1}$ region is often assigned to rocking vibrational modes of Gallium and Germanium in their polyhedra units. The intermediate frequency window between 400 – 600 $cm^{-1}$ is mainly characteristic of a combination of stretching $\nu(T^{[4]} – O – T^{[4]})$ and $\delta$ $(T^{[4]} – O – T^{[4]})$ bending modes of an oxygen surrounded by two tetrahedral units (T = gallium, germanium) linked by their corners [8], [28]. Looking first the low frequency region, one observes mainly in the Infra-Red spectrum that the introduction of Yttrium oxide leads to decrease the vibrational signature of the mode located at ~ 330 $cm^{-1}$ for the benefit of an increase of the signature around ~ 430 $cm^{-1}$. This changes can be mainly attributed to the substitution of Lanthanum by Yttrium. The intermediate regions is slightly modified as shown in both Raman and IR spectra. This suggests that the glass network mainly made with T – O – T bridges

is relatively little affected depending on the kind of the rare – earth present in the glass. The most important spectral variations arise in the high frequency regions. According to the similar Raman and FTIR spectral variations, two main effects upon the introduction of yttrium oxide are observed which are ***(i)*** an increase of the vibrational band intensities located around ~ 644 $cm^{-1}$ and ***(ii)*** a shift of the main Raman band from ~ 813 $cm^{-1}$ to ~ 800 $cm^{-1}$ m meanwhile a shift from ~ 744 $cm^{-1}$ to ~ 739 $cm^{-1}$ of Infra-Red one. Regarding the first item, the spectral variations assignation of the vibrational activities in the ~ 600 - 700 $cm^{-1}$ remains complex and a little explored. Yoshimoto *et al.* [26] have assigned those vibrational mode to a various Ga – O bridges involved in $GaO_x$ environment. Referring to the SSNMR results obtained, one might assign mostly those spectral change to the increase of $GaO_5$ units. In addition to that, based on the literature on alumino-silicates glasses [18], [19], one can propose that the increase in high field strength cation in the glass composition breaks the well-known Lowenstein rules, stating preference for the avoidance of $O_3Al – O – AlO_3$ bridges. We believe that similar rule could occur and therefore be relaxed in the presence of rare – earth germano – gallate glasses. Therefore, we also propose to assign those modes to Ga – O – Ga links with gallium in tetrahedral or pentahedral environment. Nonetheless, further structural investigations such as DFT calculations will need to be performed in order to confirm the latter assignment. The highest vibrational modes regarding the second item can be mainly assigned to $Q_2$ (~ 744 $cm^{-1}$) and $Q_3$ (~ 813 $cm^{-1}$) germanate units [28]. The frequency shift observed in both Raman/IR while introducing yttrium oxide with respect to lanthanum oxide results is partly due the change in the reduced frequency constant. This could be mostly explained by the heavier mass of lanthanum element as compared to yttrium one.

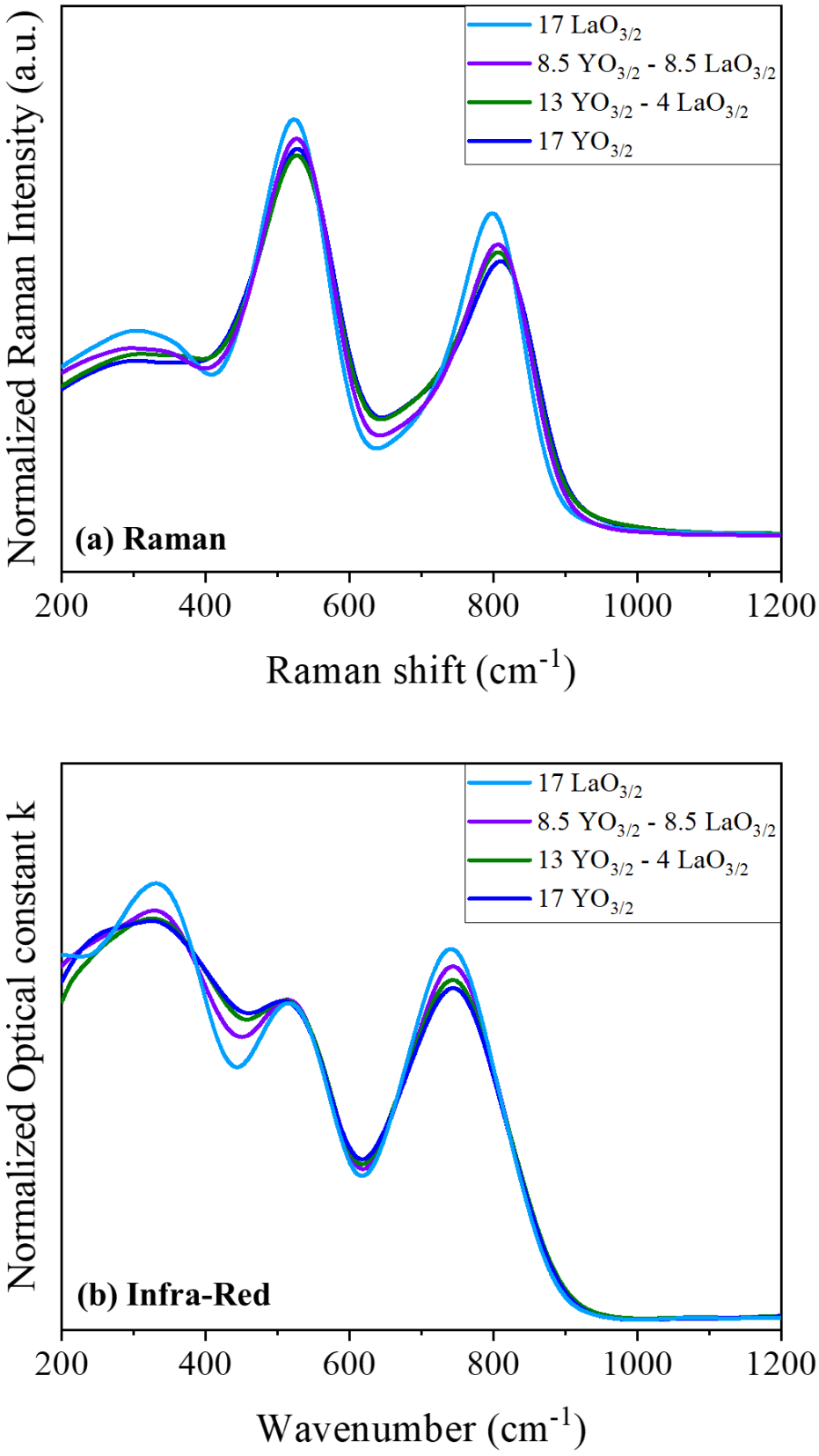


**<u>Figure 10:</u> Area normalized (a) Raman and (b) FTIR spectra of the investigated glass series**

The optical fiber drawing of germano-gallate HMO glasses is of great interests since those gallium-rich original new glass compositions exhibit superior assets such as excellent thermal and mechanical properties as well as interesting nonlinear properties while being transparent up to ~5.5 µm [7]. Nonetheless, their shaping has remained a considerable challenge due to the apparition of the surface crystallization of solid solutions during the optical fiber drawing process, preventing therefore further technological applications. Herein, we resolve this issue while understanding the key role of yttrium oxide disabling the langasite-type appearance. We believe that this study paves the way to develop a panel of robust active optical fiber since we have shown that the introduction of high field of rare – earth favor the ability to extend germano – gallate glasses compositions and hence introduce further IR emitting dopants in a relatively large amount while exhibiting a relatively small ionic radius such as $Yb^{3+}$, $Tm^{3+}$, $Er^{3+}$, $Ho^{3+}$, $Dy^{3+}$. For the purpose of understanding the effect of yttrium oxide on the ability to draw gallium-rich optical glasses as optical fibers, investigations of crystallization behaviors, properties and local glass structure depending on the nature of the rare – earth (La or Y) were successful. The crystallization studies have evidenced the ability of $YO_{3/2}$ to prevent the devitrification of langasite-type phases since those ones were mostly synthesized with a cation exhibiting a relatively large ionic radius. Meanwhile, in agreement with both $^{71}Ga$ solid-state Nuclear Magnetic Resonance (SSNMR) combined with Infrared and Raman vibrational response, we have shown that the introduction of $YO_{3/2}$ leads to change the local gallium coordination from $GaO_4$ to $GaO_5$ units. This change in local glass structure is of major importance since it increases the covalence nature of the glass network and then improve the glass transition values of the $YO_{3/2}$-rich glasses and thus also the Knoop micro-hardness [18]. This structural description holds well with the variation of the thermal and physical properties. Those results merge into showing that $YO_{3/2}$-rich glasses as a key element for the development of new gallium- rich robust mid-infrared transparent optical fibers.

**Conclusion.** Herein, we report on the key role played $YO_{3/2}$ ions as compared to $LaO_{3/2}$ to prevent the surface crystallization and therefore enabling the shaping of gallium-rich germanate optical fibers. Taking advantage of structural information from vibrational spectroscopies (Raman/Infrared) and $^{71}Ga$ Solid-State Nuclear Magnetic Resonance (SSNMR), we further demonstrate that the higher field cation of $YO_{3/2}$ leads to change the local gallium coordination from $GaO_4$ to $GaO_5$ units, therefore improving thermal and mechanical properties. These results

provide insights in the shaping of new optical fibers of mid-infrared vitreous materials having a strong technological potential in optics and photonics.

**Acknowledgments.**

We acknowledge the financial support from CNRS (IRP LuMAQ), the French National Research Agency (ANR) (ANR-18-CE08-0004-02) and the Region Nouvelle Aquitaine (project AAPR2020-2019-8193110). We also acknowledge the financial support from the Grand Research Program « LIGHT » Idex University of Bordeaux, and the Graduate program « EUR Light S&T » PIA3 ANR-17-EURE-0027.

**References.**

[1] K. C. Kao and G. A. Hockham, 'Dielectric-fibre surface waveguides for optical frequencies', *Proceedings of the Institution of Electrical Engineers*, vol. 113, no. 7, pp. 1151–1158, Jul. 1966, doi: 10.1049/piee.1966.0189.

[2] A. Jha, *Inorganic glasses for photonics: fundamentals, engineering, and applications*. New Jersey: John Wiley & Sons, Inc, 2016.

[3] G. Tao *et al.*, 'Infrared fibers', *Advances in Optics and Photonics*, vol. 7, no. 2, p. 379, Jun. 2015, doi: 10.1364/AOP.7.000379.

[4] P. D. Dragic, M. Cavillon, and J. Ballato, 'Materials for optical fiber lasers: A review', *Applied Physics Reviews*, vol. 5, no. 4, p. 041301, Dec. 2018, doi: 10.1063/1.5048410.

[5] A. B. Seddon *et al.*, 'Mid-infrared integrated optics: versatile hot embossing of mid-infrared glasses for on-chip planar waveguides for molecular sensing', *Optical Engineering*, vol. 53, no. 7, p. 071824, Jun. 2014, doi: 10.1117/1.OE.53.7.071824.

[6] S. S. Bayya, B. B. Harbison, J. S. Sanghera, and I. D. Aggarwal, 'BaO□Ga2O3□GeO2 glasses with enhanced properties', *Journal of Non-Crystalline Solids*, vol. 212, no. 2, pp. 198–207, Jun. 1997, doi: 10.1016/S0022-3093(96)00658-8.

[7] C. Strutynski *et al.*, 'Heavy-oxide glasses with superior mechanical assets for nonlinear fiber applications in the mid-infrared', *Opt. Mater. Express*, vol. 11, no. 5, p. 1420, May 2021, doi: 10.1364/OME.417699.

[8] T. Skopak *et al.*, 'Structure and Properties of Gallium-Rich Sodium Germano-Gallate Glasses', *The Journal of Physical Chemistry C*, vol. 123, no. 2, pp. 1370–1378, Jan. 2019, doi: 10.1021/acs.jpcc.8b08632.

[9] T. Skopak *et al.*, 'Properties, structure and crystallization study of germano-gallate glasses in the Ga2O3-GeO2-BaO-K2O system', *Journal of Non-Crystalline Solids*, vol. 514, pp. 98–107, Jun. 2019, doi: 10.1016/j.jnoncrysol.2019.02.028.

[10] T. Guérineau, A. Fargues, Y. Petit, E. Fargin, and T. Cardinal, 'The influence of potassium substitution for barium on the structure and property of silver-doped germano-gallate glasses', *Journal of Non-Crystalline Solids*, vol. 566, p. 120889, Aug. 2021, doi: 10.1016/j.jnoncrysol.2021.120889.

[11] X. Wen *et al.*, 'Highly Tm3+ doped germanate glass and its single mode fiber for 2.0 μm laser', *Scientific Reports*, vol. 6, no. 1, Apr. 2016, doi: 10.1038/srep20344.

[12] T. Guérineau *et al.*, 'Extended germano-gallate fiber drawing domain: from germanates to gallates optical fibers', *Opt. Mater. Express*, vol. 9, no. 6, p. 2437, Jun. 2019, doi: 10.1364/OME.9.002437.

[13] D. Massiot *et al.*, 'Modelling one- and two-dimensional solid-state NMR spectra', *Magnetic Resonance in Chemistry*, vol. 40, no. 1, pp. 70–76, 2002, doi: 10.1002/mrc.984.

[14] B. A. Maksimov *et al.*, 'Absolute structure of La3Ga5SiO14 langasite crystals', *Crystallogr. Rep.*, vol. 50, no. 5, pp. 751–758, Sep. 2005, doi: 10.1134/1.2049391.

[15] B. V. Mill and Y. V. Pisarevsky, 'Langasite-type materials: from discovery to present state', in *Proceedings of the 2000 IEEE/EIA International Frequency Control Symposium and Exhibition (Cat. No.00CH37052)*, Jun. 2000, pp. 133–144. doi: 10.1109/FREQ.2000.887343.

[16] P. Florian, N. Sadiki, D. Massiot, and J. P. Coutures, '$^{27}$ Al NMR Study of the Structure of Lanthanum- and Yttrium-Based Aluminosilicate Glasses and Melts', *J. Phys. Chem. B*, vol. 111, no. 33, pp. 9747–9757, Aug. 2007, doi: 10.1021/jp072061q.

[17] A. Jaworski, B. Stevensson, and M. Edén, 'The Bearings from Rare-Earth (RE = La, Lu, Sc, Y) Cations on the Oxygen Environments in Aluminosilicate Glasses: A Study by Solid-State $^{17}$ O NMR, Molecular Dynamics Simulations, and DFT Calculations', *The Journal of Physical Chemistry C*, vol. 120, no. 24, pp. 13181–13198, Jun. 2016, doi: 10.1021/acs.jpcc.6b02032.

[18] S. Iftekhar *et al.*, 'Properties and Structures of $RE_2O_3$–$Al_2O_3$–$SiO_2$ (RE = Y, Lu) Glasses Probed by Molecular Dynamics Simulations and Solid-State NMR: The Roles of Aluminum and Rare-Earth Ions for Dictating the Microhardness', *J. Phys. Chem. C*, vol. 116, no. 34, pp. 18394–18406, Aug. 2012, doi: 10.1021/jp302672b.

[19] M. Edén, '27Al NMR Studies of Aluminosilicate Glasses', in *Annual Reports on NMR Spectroscopy*, vol. 86, Elsevier, 2015, pp. 237–331. doi: 10.1016/bs.arnmr.2015.04.004.

[20] C. I. Merzbacher and D. A. McKeown, 'X-ray absorption studies of Ge and Ga environments in BaO□Ga2O3□GeO2 glasses', *Journal of Non-Crystalline Solids*, vol. 162, no. 1–2, pp. 81–100, Sep. 1993, doi: 10.1016/0022-3093(93)90743-H.

[21] P. L. Higby and I. D. Aggarwal, ‘Properties of barium gallium germanate glasses’, *Journal of Non-Crystalline Solids*, vol. 163, no. 3, pp. 303–308, Dec. 1993, doi: 10.1016/0022-3093(93)91308-P.

[22] S. M. Bradley, R. F. Howe, and R. A. Kydd, ‘Correlation between27Al and71Ga NMR chemical shifts’, *Magn. Reson. Chem.*, vol. 31, no. 10, pp. 883–886, Oct. 1993, doi: 10.1002/mrc.1260311002.

[23] C. O. Areán, M. R. Delgado, V. Montouillout, and D. Massiot, ‘Synthesis and Characterization of Spinel-Type Gallia-Alumina Solid Solutions’, *Z. anorg. allg. Chem.*, vol. 631, no. 11, pp. 2121–2126, Aug. 2005, doi: 10.1002/zaac.200570027.

[24] D. Massiot *et al.*, ‘71Ga NMR of reference GaIV, GaV, and GaVI compounds by MAS and QPASS, extension of galliumraluminum NMR parameter correlation’, p. 11, 1999.

[25] T. Schaller and J. F. Stebbins, ‘The Structural Role of Lanthanum and Yttrium in Aluminosilicate Glasses: A $^{27}$ Al and $^{17}$ O MAS NMR Study’, *J. Phys. Chem. B*, vol. 102, no. 52, pp. 10690–10697, Dec. 1998, doi: 10.1021/jp982387m.

[26] K. Yoshimoto *et al.*, ‘Principal Vibration Modes of the $La_2O_3$–$Ga_2O_3$ Binary Glass Originated from Diverse Coordination Environments of Oxygen Atoms’, *J. Phys. Chem. B*, vol. 124, no. 24, pp. 5056–5066, Jun. 2020, doi: 10.1021/acs.jpcb.0c02147.

[27] T. Skopak *et al.*, ‘Structure-properties relationship study in niobium oxide containing GaO3/2-LaO3/2-KO1/2 gallate glasses’, *Materials Research Bulletin*, vol. 112, pp. 124–131, Apr. 2019, doi: 10.1016/j.materresbull.2018.12.007.

[28] F. Calzavara *et al.*, ‘Glass forming regions, structure and properties of lanthanum barium germanate and gallate glasses’, *Journal of Non-Crystalline Solids*, vol. 571, p. 121064, Nov. 2021, doi: 10.1016/j.jnoncrysol.2021.121064.

[29] G. S. Henderson, L. G. Soltay, and H. M. Wang, ‘Q speciation in alkali germanate glasses’, *Journal of Non-Crystalline Solids*, vol. 356, no. 44–49, pp. 2480–2485, Oct. 2010, doi: 10.1016/j.jnoncrysol.2010.03.023.

[30] K. Yoshimoto, A. Masuno, M. Ueda, H. Inoue, H. Yamamoto, and T. Kawashima, ‘Low phonon energies and wideband optical windows of La2O3-Ga2O3 glasses prepared using an aerodynamic levitation technique’, *Scientific Reports*, vol. 7, no. 1, Dec. 2017, doi: 10.1038/srep45600.